Available online at www.sciencedirect.com
ScienceDirect
Trans. Nonferrous Met. Soc. China 31(2021) 2570−2584
Transactions of Nonferrous Metals Society of China
www.tnmsc.cn

Effect of Si content on interfacial reaction and properties between solid steel and liquid aluminum

Tian-peng ZOU[1], Gao-yang YU[1], Shu-hai CHEN[1], Ji-hua HUANG[1], Jian YANG[1], Zhi-yi ZHAO[1], Ji-ping RONG[1], Jin YANG[2]

1. School of Materials Science and Engineering, University of Science and Technology Beijing, Beijing 100083, China;
2. School of Materials Engineering, Shanghai University of Engineering Science, Shanghai 201620, China

Received 16 September 2020; accepted 9 April 2021

Abstract: The effect of Si content on the microstructures and growth kinetics of intermetallic compounds (IMCs) formed during the initial interfacial reaction (<10 s) between solid steel and liquid aluminum was investigated by a thermophysical simulation method. The influence of Si addition on interfacial mechanical properties was revealed by a high-frequency induction brazing. The results showed that IMCs layers mainly consisted of η-Fe_2Al_5 and θ-Fe_4Al_{13}. The addition of Si reduced the thickness of the IMCs layer. The growth of the η phase was governed by the diffusion process when adding 2 wt.% Si to the aluminum melt. When 5 wt.% or 8 wt.% Si was added to aluminum, the growth was governed by both the diffusion process and interfacial reaction, and ternary phase τ_1/τ_9-$(Al,Si)_5Fe_3$ was formed in the η phase. The apparent activation energies of the η phase decreased gradually with increasing Si content. The joint with pure aluminum metal had the highest tensile strength and impact energy.

Key words: intermetallic compounds; Si content; solid steel; liquid aluminum; interfacial reaction; mechanical properties

1 Introduction

Steel/Al hybrid structure has great application prospects in many industrial fields because it integrates the advantages of those two widely used metals. For example, steel/Al hybrid structure can reduce the mass of automobile bodies as well as maintain a certain structure performance, which contributes to energy saving and emission reduction. In addition, aluminization produces a surface with improved oxidation resistance and hot corrosion resistance, thus extending the service life and temperature limits of the low carbon steel. However, it is hard to avoid the formation of intermetallic compounds (IMCs) such as θ-Fe_4Al_{13}, η-Fe_2Al_5, and ζ-$FeAl_2$ due to the interfacial reaction between solid steel and liquid aluminum [1,2]. These IMCs badly deteriorate the mechanical properties of solid steel/liquid Al interfacial structure. Thus, the interfacial reaction between solid steel and liquid aluminum remains an essential problem to affect the bonding quality and coating quality. Researches on steel/Al interfacial reaction process and the microstructure of IMCs are of great significance to improve mechanical properties of steel/Al joint, develop new joining methods, and promote the application of steel/Al hybrid structure in the industry [3−7].

Many researchers have suggested that the reaction products between solid steel and liquid pure aluminum were mainly composed of the finger-

Corresponding author: Shu-hai CHEN, Tel/Fax: +86-10-62334859, E-mail: shchen@mater.ustb.edu.cn, shchenhit@gmail.com
Tian-peng ZOU and Gao-yang YU contributed equally to this work.
DOI: 10.1016/S1003-6326(21)65676-5

like η phase adjacent to steel and needle-like θ phase adjacent to aluminum. There was a high concentration of vacancies along the *c*-axis of the η phase, which induced the rapid growth of η phase [8]. The growth of the η phase obeyed a parabolic law with longer reaction time (tens of seconds to minutes) [9], and θ phase precipitated during the cooling process [10]. In recent years, it was found that the composition of IMCs layers might change under different reaction conditions. For example, very thin intermetallic phases κ-$AlFe_3C$ and β'-AlFe were observed between steel and η phase in the interdiffusion of solid steel and solid aluminum [1]. In addition, FeAl and Fe_3Al were formed in the coatings of hot-dip aluminizing steel by high- temperature diffusion-treatment [11].

The formation mechanism and growth kinetics of IMCs were also the research hotspots of steel/Al interfacial reaction [10,12−15]. Some researches suggested that the IMCs had a fast growth process in the initial stage of reaction, when the growth of η phase deviated from the parabolic law, namely, the growth was not only governed by the diffusion process [12−15]. RONG et al [15] studied the growth kinetics of η phase between solid steel and molten aluminum in the initial stage (reaction time <10 s). They found that the growth of average thickness of η phase was controlled by both the diffusion process and interfacial reaction.

Adding alloying elements is an important way to control the interfacial reaction [1,16−19]. Researchers have found that the addition of Si to aluminum melt could reduce the thickness of brittle IMCs as well as change the composition and morphology of IMCs [1,9,20−23]. However, the effect mechanism of Si on the formation and growth of IMCs was not clarified. NICHOLLS [20] and YIN et al [21] concluded that Si atoms would occupy the vacancies in the η phase, which suppressed the fast growth of η phase. LEMMENS et al [22] deduced that the growth reduction of η phase was attributed to the enrichment of Si at grain boundaries and phase boundaries of IMCs. ZHANG et al [23] suggested that the reduction of the activity value of Al caused by Si addition suppressed the interfacial reaction between Fe and Al. LEMMENS et al [9] concluded that the formation of Fe−Al−Si ternary phases might act as diffusion barriers.

The interfacial reaction between steel and aluminum is influenced by several factors such as reaction temperature, reaction time, and Si content in the aluminum melt. To simplify the experiment, researchers paid more attention to a small temperature range [1,9] or a small content range of Si [21,24−27]. SPRINGER et al [1] and LEMMENS et al [9] observed that excessive Si addition might increase the thickness of IMCs when the reaction temperature was relatively low. YIN et al [21] investigated the effect of Si content (from 0 to 3 wt.%) on the growth kinetics of η phase at a relatively wide temperature range (from 700 to 850 °C). They also observed that the apparent activation energy of the η phase decreased with increasing Si content. SPRINGER et al [1], LEMMENS et al [9], and YIN et al [21] suggested that when Si was added to the aluminum melt, the growth of η phase still obeyed a parabolic law in tens of seconds to minutes. It was noteworthy that YIN et al [21] suggested that the growth of the η phase deviated from the parabolic law in the initial stage. They suggested that there was an interface control reaction at the beginning of the process.

The above investigations indicate that the effect mechanism of Si on steel/Al interfacial reaction is still controversial. Lack of systematic research on the effects of different Si contents on the interfacial reaction and mechanical properties makes it difficult to understand the effect mechanism of Si element. These researches are of great significance to control the mechanical properties of the interface between steel and aluminum.

In this study, the effect of Si on the interfacial reaction between solid steel and liquid aluminum in the initial reaction stage (reaction time <10 s) at the temperatures of 700−900 °C was investigated by a Gleeble 1500 thermophysical simulator. Based on the thermophysical simulation results, the formation mechanism and growth kinetics of IMCs were analyzed. To investigate the effect of Si addition in aluminum-based filler metals on the interfacial mechanical properties under different thermal cycle processes, the Q235 steel brazing experiment was conducted by a high-frequency induction brazing method. The experimental results contributed to guide the selection of reaction temperature, reaction time, and Si content during the steel−aluminum brazing or hot-dip aluminizing process.

2 Experimental

2.1 Thermophysical simulation experiment

A commercial Q235 steel rod (0.19% C, 0.80% Mn, 0.04% Si, 0.33% Al, balanced Fe, in wt.%) with a diameter of 10 mm was cut to a length of 90 mm. A keyway was machined in the center of the steel rod. Another two Q235 steel sheets with the same chemical composition were marked as A (6 mm × 5 mm × 1 mm) and B (see Fig. 1), respectively. Pure Al (99.99 wt.%) and high-purity Si (99.99 wt.%) were used to smelt Al−Si alloys by an arc melting method. The Si contents were 0, 2, 5, and 8 wt.%, respectively.

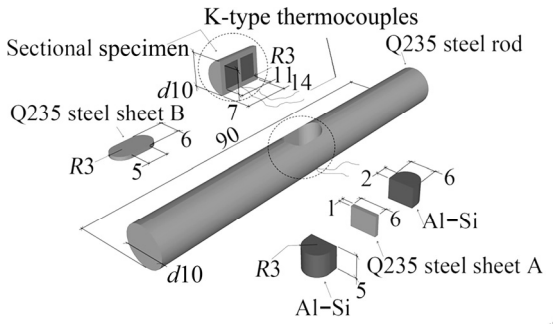

Fig. 1 Diagram of sample dimensions and assemblage in thermophysical simulation experiment (Unit: mm)

Greases and residues on the surface of steel sheets and the keyway were removed with acetone before the experiment. The Al−Si alloy blocks were immersed in 10% NaOH solution for 3 min to remove greases and oxides, then put in 10% HNO_3 solution for 10 s. The Al−Si alloy blocks were rinsed with deionized water and dried with a hair drier after chemical polishing treatment. The Nocolok flux mixed with alcohol was evenly spread over the surface of Q235 steel sheets, Al blocks, and Al−Si alloy blocks.

The steel sheet A was clamped between two freshly processed Al−Si alloy blocks (or two Al blocks) in the keyway of the steel rod. Because the presence of oxygen could influence the growth of IMCs [28,29], the steel sheet B was used to seal the keyway to keep out the air and to prevent the liquid from splashing, which could minimize the effect of oxygen. Figure 1 shows the dimensions and assemblages of steel sheets, steel rod, and Al−Si alloy blocks (or Al blocks). The assemblage of steel sheets, Al−Si alloy blocks, and the keyway was an interference fit.

A thermophysical simulator, Gleeble 1500, with the highest heating rate of 10000 K/s was used to heat the sample. The K-type thermocouples were welded at the bottom of the keyway to measure and control the temperature. An automatic water-spray nozzle controlled by the system was added to cool the specimen. Figure 2 shows the typical temperature curve, which shows that the measuring curve is in good agreement with the preset curve. The specimen was preheated to 600 °C holding for 5 s. The interdiffusion influence of the preheating process was ignored because of the relatively low atoms diffusion rate between solid/solid and solid/semi-solid interdiffusion processes. The method shows high-precision control for the solid steel/liquid Al−Si alloys interfacial reaction. Thus it is suitable to investigate the non-equilibrium interfacial reaction and its kinetics during short durations (a few seconds). Further details about this experiment were provided in the previous publication [15].

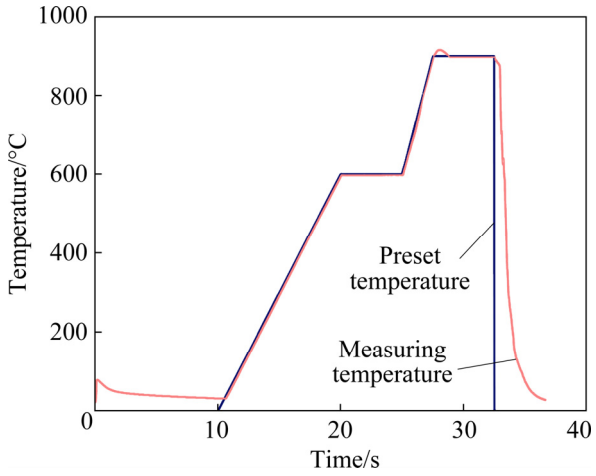

Fig. 2 Curve of temperature with time in thermophysical simulation experiment

The peak temperatures were set to be 700, 750, 800, 850, and 900 °C, respectively. The holding time was 0, 1, 3, 5, 7, and 9 s, respectively. Though the heating rate and cooling rate were quite high, it was inevitable that interfacial reaction occurred during the heating and cooling process. To reduce the error, the thickness of the η phase obtained during the isothermal process was selected in the kinetics analysis, and the thickness was calculated by subtracting the thickness of η phase of 0 s from that of 1, 3, 5, 7, and 9 s, respectively.

2.2 Interfacial mechanical properties experiment

The brazing experiments were conducted to investigate the mechanical properties of the interface. The Q235 low-carbon steel was selected as the base material. The pure aluminum, Al−5wt.%Si, Al−8wt.%Si, and Al−12wt.%Si were selected as filler metals. The Nocolok flux was coated homogeneously on the surface of steel and aluminum alloys. The sample dimensions and assemblage are shown in Fig. 3. Butt brazing was carried out by a high-frequency induction heating source under argon protection. The 304 stainless steel sheet with a thickness of 0.3 mm was used for presetting a gap so that liquid filler metal could wet the surface of steel successfully.

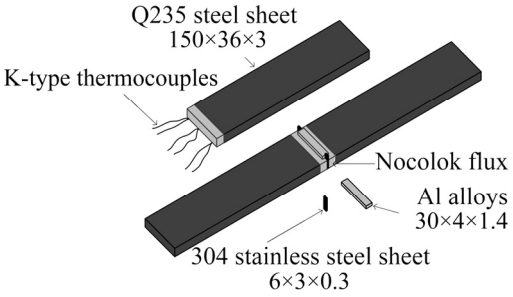

Fig. 3 Diagram of sample dimensions and assemblage in brazing experiment (Unit: mm)

The heating temperature was slightly higher than the liquidus temperature of filler metal and measured by the K-type thermocouples. The heating immediately stopped when the actual temperature reached the preset heating temperature of aluminum alloys. Table 1 lists the liquidus temperature of aluminum alloys and the preset heating temperature. The heating rate was 15 °C/s. The specimen was cooled in the air after reaching the peak temperature.

Table 1 Temperature used in brazing experiment

Brazing filler metal	Liquidus temperature/°C	Heating temperature/°C
Pure Al	660	680
Al−5wt.%Si	630	650
Al−8wt.%Si	610	640
Al−12wt.%Si	577	610

2.3 Microstructure characterization and mechanical properties test

After the thermophysical simulation, a typical cross-section of the specimen was cut and standard metallographic preparation procedures were carried out. The dimensions of the cross-section specimen are shown in Fig. 1. For the brazing test, the metallographic specimen (10 mm × 5 mm × 3 mm), the tensile specimen (130 mm × 10 mm × 3 mm), and the impact specimen (55 mm × 10 mm × 3 mm) were cut at the brazing seam by line cutting. No notch was designed on the impact specimen because the brittleness of IMCs in butt joints was higher than parent metals, which caused the specimen to easily fracture at the IMCs interface. The microstructures of IMCs were observed via a scanning electron microscope (SEM) equipped with energy dispersive spectroscopy (EDS). The thickness of IMCs was measured by image processing methods. The tensile and impact tests were carried out by a tensile testing machine and an impact testing machine, respectively.

3 Results

3.1 Thermophysical simulation

3.1.1 Microstructure

Figure 4 shows the SEM images of IMCs formed at 900 °C for 7 s. The image of IMCs between pure aluminum and steel is shown in Fig. 4(a). According to the EDS results, the reaction products consisted of η-Fe_2Al_5 and θ-Fe_4Al_{13}. The η phase exhibited a finger-like morphology towards the steel side. The θ phase presented a serrated shape towards aluminum or a free state within the aluminum. The boundaries between the two phases were highlighted by white dashed lines. The thickness of the η phase was much larger than that of the θ phase. An obvious crack in the η phase was observed, which indicated the brittleness of the η phase.

Figure 4(b) shows the interfacial morphology when the solid steel reacted with the liquid Al−2wt.%Si. The thickness of the η phase decreased and the interface between η phase and steel became flatter compared with the reaction between pure aluminum and steel. The θ phase adhered to η phase still exhibited irregular serrated shape, and the free θ phase increased and grew. After the Si content in the aluminum melt increased to 5 or 8 wt.%, the interface between the η phase and steel remained a smooth morphology and the free θ phase further increased, as shown in Figs. 4(c, d). It was noted that a new punctate phase

was observed in η phase when the Si content exceeded 5 wt.%, and the distribution of this punctate phase became wider with increasing Si content. This new phase was identified as Fe−Al−Si ternary phase τ_1/τ_9-$(Al, Si)_5Fe_3$ according to the morphology, EDS-analysis results, and previous researches [21,30,31].

Figure 5 shows the effect of reaction temperature and time on the thickness and morphology of IMCs when Si content in the aluminum melt was 5 wt.%. The micrographs of reaction layers formed at 900 °C for 1 s and 9 s are respectively shown in Figs. 5(a, b). With prolonging the reaction time, the thickness of the η phase increased and the θ phase grew. Figure 5(c) shows the SEM image of reaction layers formed at 850 °C for 9 s. Compared Fig. 5(b) with Fig. 5(c), it was shown that thicker η phase and bigger θ phase formed at higher temperatures.

3.1.2 Growth kinetics of η phase

According to Fig. 4, the influence of Si content in the aluminum melt on the thickness of the η phase was greater than that on the thickness of the θ phase adhered to the interface, which was in accordance with the study of LEMMENS et al [9]. Thus, the present study mainly focused on the effect of Si on the growth kinetics of the η phase.

The growth kinetics of the η phase was investigated according to the results of the thermophysical simulation experiment. The growth kinetics can be expressed as

$$X-X_0=\Delta X=K(T)t^n \quad (1)$$

And Eq. (1) is calculated as

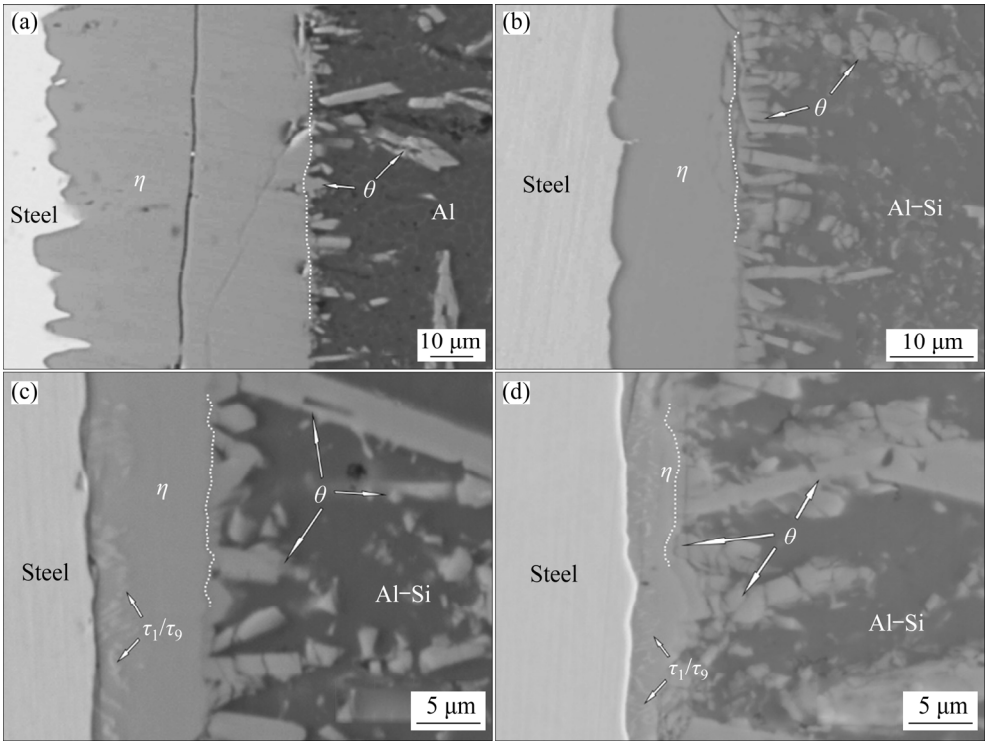

Fig. 4 Typical SEM images of IMC layers formed at 900 °C for 7 s: (a) Al; (b) Al−2wt.%Si; (c) Al−5wt.%Si; (d) Al−8wt.%Si

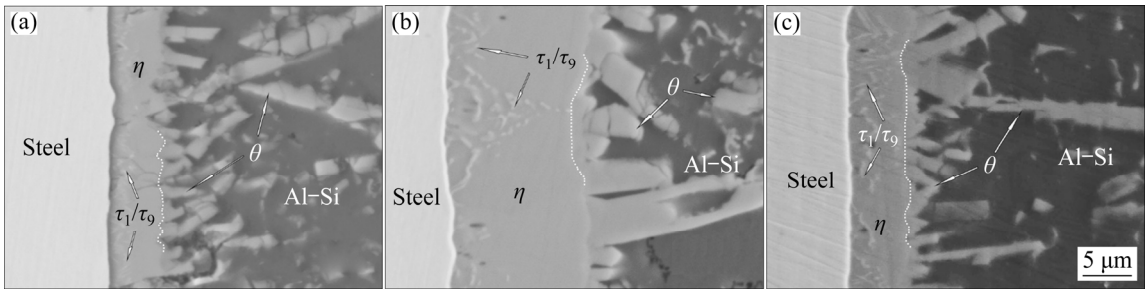

Fig. 5 Typical micrographs of reaction layers with 5 wt.% Si at different temperatures for different holding time: (a) 900 °C, 1 s; (b) 900 °C, 9 s; (c) 850 °C, 9 s

$$\ln(X-X_0)=\ln(\Delta X)=n\ln t+\ln[K(T)] \quad (2)$$

where X is the average thickness (μm) of η phase when holding time t is 1−9 s, X_0 is the average thickness (μm) of η when t is 0 s, T is the temperature (K), $K(T)$ is the growth rate constant, and the time exponent n is a constant. The growth is controlled by the interfacial reaction when n=1, whereas the growth is controlled by the diffusion process when n=0.5 [12]. When the contents of Si are 0, 2, 5, and 8 wt.%, the fitting curves of $\ln(\Delta X)$ and $\ln t$ at 750 °C are shown in Fig. 6. Table 2 summarizes the slopes of fitting curves with different Si contents at different temperatures, which are the time exponent n according to Eq. (2). To simplify the mathematical model in the present work, the average time exponent was used to deduce the growth kinetics of η phase, and the average values of n were around 0.77 (Al), 0.52 (Al−2wt.%Si), 0.76 (Al−5wt.%Si), and 0.86 (Al−8wt.%Si).

According to Eq. (1), the time exponent n can be verified by the results of the fitting curves between t^n and ΔX. The slopes, namely the values of $K(T)$, and the intercepts of the fitting curves with different Si contents at different temperatures are respectively listed in Tables 3 and 4. The intercepts listed in Table 4 show that ΔX is near to zero when t=0 s, which is in accordance with the reality and indicates that this method is exact to investigate the initial stage of the interfacial reaction between steel and aluminum.

The relationship between temperature T and the growth rate constant $K(T)$ is in accordance with the Arrhenius equation:

$$K(T)=K_0\exp\left(-\frac{E_a}{RT}\right) \quad (3)$$

And Eq. (3) is calculated as

$$\ln[K(T)]=-\frac{E_a}{RT}+\ln K_0 \quad (4)$$

where K_0 is the pre-exponential factor and is a constant, E_a is the apparent activation energy (J) for the growth of the η phase, and R is the gas constant 8.314 J/(K·mol). Figure 7 shows the fitting curves between $1/T$ and $\ln[K(T)]$ (the data points at 900 °C are excluded when Si contents in the aluminum melt are 0 and 2 wt.%). The slopes of fitting lines

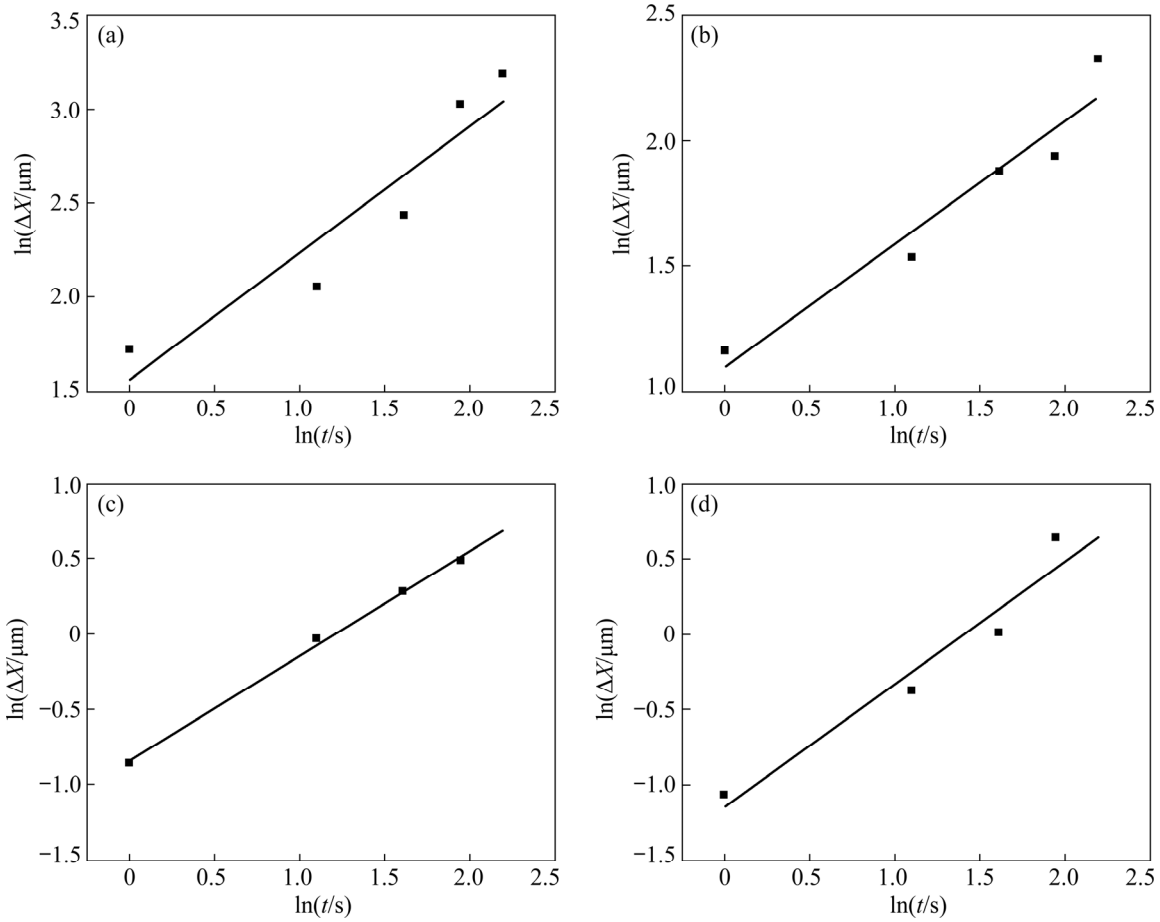

Fig. 6 Linear fitting curves of $\ln(\Delta X)$ and $\ln t$ at 750 °C: (a) Al; (b) Al−2wt.%Si; (c) Al−5wt.%Si; (d) Al−8wt.%Si

Table 2 Time exponent n of growth kinetics of η phase with different Si contents

Temperature/ °C	Time exponent, n			
	0 wt.%	2 wt.%	5 wt.%	8 wt.%
700	0.73	0.49	0.66	0.80
750	0.67	0.49	0.70	0.82
800	0.75	0.49	0.82	0.79
850	0.85	0.59	0.80	0.91
900	0.83	0.55	0.82	0.97
Average	0.77	0.52	0.76	0.86

Table 3 Slope ($K(T)$) of linear fitting curves of ΔX and t^n with different Si contents

Temperature/ °C	$K(T)$			
	0 wt.%	2 wt.%	5 wt.%	8 wt.%
700	1.90	1.69	0.27	0.32
750	4.49	3.03	0.35	0.34
800	7.97	4.08	0.71	0.22
850	9.63	4.57	0.76	0.36
900	10.68	3.75	0.87	0.39

Table 4 Intercept (fitting error of ΔX) of linear fitting curves of ΔX and t^n with different Si contents

Temperature/ °C	Fitting error of ΔX			
	0 wt.%	2 wt.%	5 wt.%	8 wt.%
700	−0.05	−0.52	0.02	0.07
750	−1.02	−0.33	0.10	−0.12
800	−0.95	−0.79	−0.45	0.11
850	−2.37	−1.34	−0.38	−0.25
900	−1.14	−1.09	−0.49	−0.29

are the values of $-E_a/R$, and the intercepts are the values of $\ln K_0$. Table 5 shows the slopes and intercepts of fitting lines in Fig. 7 and summarizes the calculated values of E_a and K_0. According to the data in Table 5, the mathematical models of X, namely the average thickness of η phase, with different Si contents in the aluminum melt are based on Eqs. (5−8):

$$X_{0\text{wt.\%Si}}=5.03722\times10^{-1}\exp(-\frac{12028.92877}{T})t^{0.77} \quad (5)$$

$$X_{2\text{wt.\%Si}}=3.22217\times10^{-3}\exp(-\frac{7250.8651}{T})t^{0.52} \quad (6)$$

$$X_{5\text{wt.\%Si}}=4.43621\times10^{-4}\exp(-\frac{7177.48311}{T})t^{0.76} \quad (7)$$

$$X_{8\text{wt.\%Si}}=7.44435\times10^{-7}\exp(-\frac{896.46138}{T})t^{0.86} \quad (8)$$

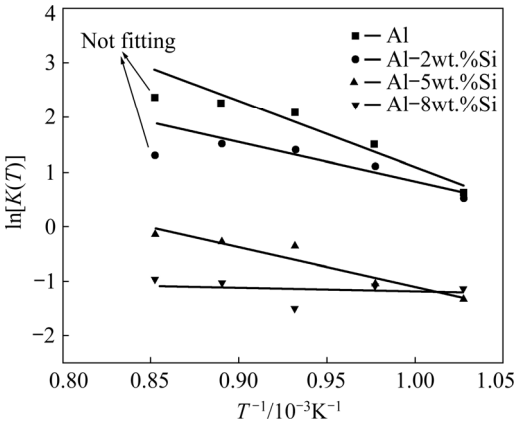

Fig. 7 Linear fitting curves between $1/T$ and $\ln[K(T)]$

Table 5 Values of slope ($-E_a/R$) and intercept ($\ln K_0$) in Fig. 7

Si content/ wt.%	$(-E_a/R)$/ K	$\ln[K_0/(\mu m\cdot s^{-n})]$	E_a/ (kJ·mol^{-1})	K_0/ (m·s^{-n})
0	−12028.92877	13.12978	100.01	5.03722×10^{-1}
2	−7250.8651	8.07781	60.28	3.22217×10^{-3}
5	−7177.48311	6.09497	59.67	4.43621×10^{-4}
8	−896.46138	−0.29513	7.45	7.44435×10^{-7}

3.2 Interfacial mechanical properties

To investigate the effect of Si content on the interfacial mechanical properties of steel/ aluminum dissimilar metals, a butt brazing of steel plates with different Al−Si filler metals was designed. The interfacial microstructure of brazing joints is shown in Fig. 8. Figure 8(a) shows the reaction layers with pure aluminum filler metal. The morphology of IMCs is similar to that in Fig. 4(a). The IMC adjacent to steel exhibited a finger-like morphology and the IMC adjacent to aluminum presented an irregular serrated or needle-like shape. Figures 8(b−d) show the micrographs of reaction layers when the Si contents in aluminum base filler metals are 5, 8, and 12 wt.%. The interface between IMCs and steel transformed to a planar morphology from a finger-like morphology. The thickness of IMCs significantly decreased. When the Si contents in filler metals were 0, 5, 8, and 12 wt.%, the average thicknesses of IMCs were 14.74, 6.98, 6.61, and 5.86 μm, respectively.

The average tensile strength of the brazing joint is shown in Fig. 9(a). The joint with pure aluminum filler metal had the highest tensile strength of 100.42 MPa. When the Si contents in filler metals were 5, 8, and 12 wt.%, tensile strengths

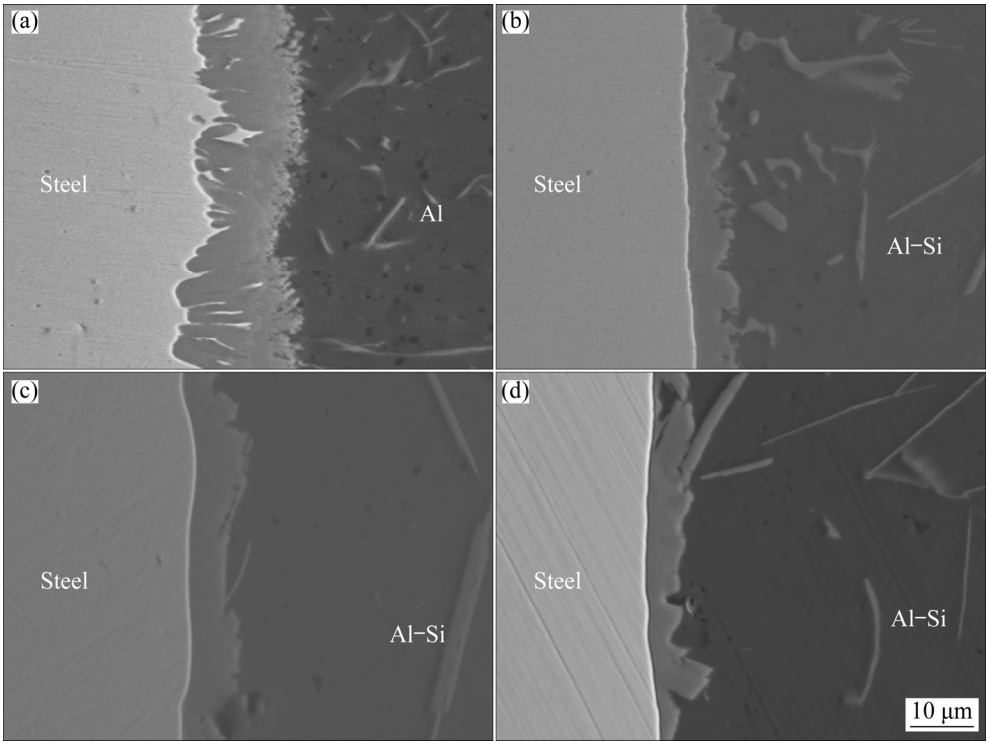

Fig. 8 Typical micrographs of brazing experiment reaction layers with different Si contents: (a) Al; (b) Al−5wt.%Si; (c) Al−8wt.%Si; (d) Al−12wt.%Si

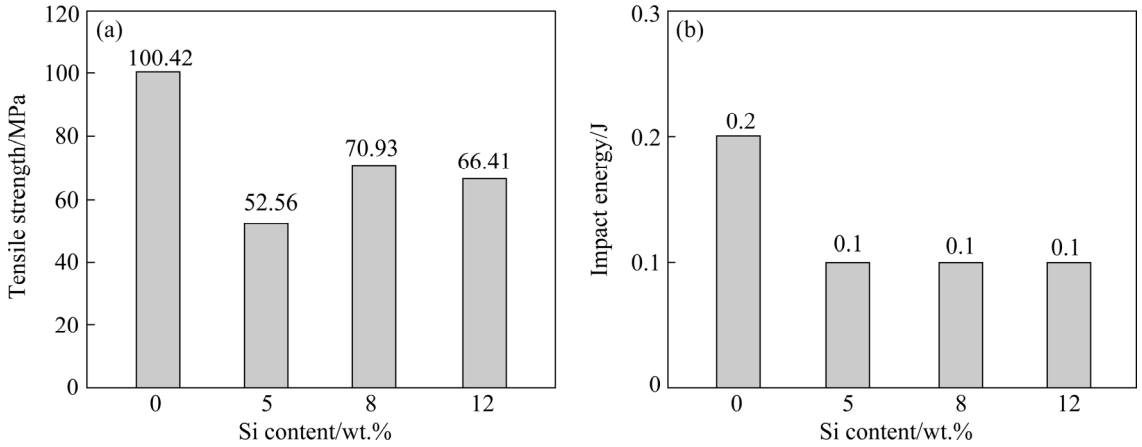

Fig. 9 Mechanical properties of brazing joints with different Si contents: (a) Tensile strength; (b) Impact energy

of joints were 52.56, 70.93, and 66.41 MPa, respectively. All the fracture surfaces were formed by brittle fracture. When the Si contents were 0, 5, and 8 wt.%, fractures occurred in both the filler metal layers and IMCs layers. When the Si content was 12 wt.%, the fracture mainly occurred in IMCs layers. The results of impact tests are shown in Fig. 9(b). The results indicated that the joint with pure aluminum filler metal had the highest impact energy of 0.2 J, compared with about 0.1 J with three Al−Si filler metals.

Figure 10 shows the tensile fracture surfaces of joints with different filler metals. There were some bulges on the fracture surfaces of joints with pure Al filler metal (Fig. 10(a)), while the fracture surfaces of joints with Al−Si filler metal were smoother (Figs. 10(b−d)).

4 Discussion

4.1 Evolution of interfacial microstructure and morphology

Figure 4(a) shows a finger-like morphology of the η phase for the interfacial reaction between pure

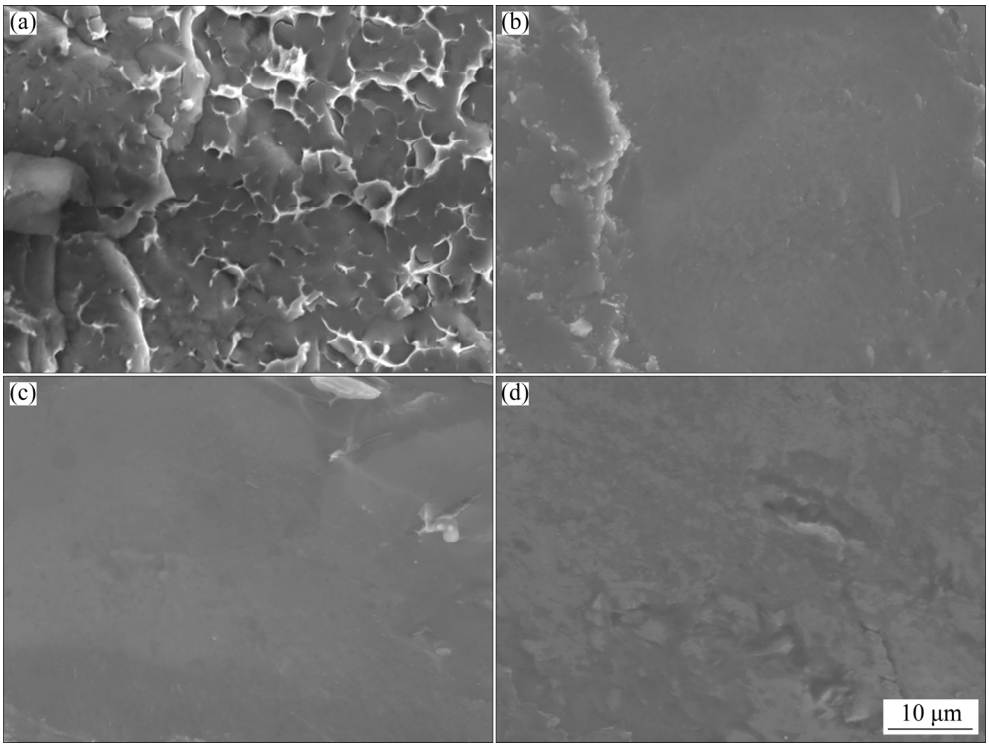

Fig. 10 Tensile fracture surfaces of brazing joints with different Si contents: (a) Al; (b) Al−5wt.%Si; (c) Al−8wt.%Si; (d) Al−12wt.%Si

aluminum and steel. This irregular morphology is the result of high concentration (near 30%) vacancies along the *c*-axis of the η phase, which provide a fast channel for atom diffusion. CHENG and WANG [8] found that the η phase preferentially grew along the [001] direction of the crystal structure, namely the *c*-axis, thereby presenting a tongue-like morphology. The θ phase adjacent to aluminum exhibited a discontinuous serrated shape. A small amount of free needle-like θ phase is distributed in the aluminum, as shown in Fig. 4(a). Previous researches considered that Fe atoms dissolving into aluminum melt precipitated in the form of θ phase in the cooling process [13], and when the temperature dropped to a certain level the Fe-containing aluminum melt transformed into eutectic structures of θ phase and Al [1]. In addition, some studies suggested that the formation of θ phase adhered to the interface was related to the interfacial reaction [10], or the reaction diffusion [12].

It can be seen from Fig. 4 that Si in the aluminum melt played an important role during the interfacial reaction between solid steel and liquid aluminum. The reduction of the thickness of the η phase was attributed to the hindrance effect of Si on the diffusion of Fe and Al atoms. Because the η phase preferential growth along the *c*-axis was impeded, the irregular finger-like morphology finally disappeared. Some researchers suggested that Si could occupy part of vacancies along the *c*-axis of the η phase [20,21]. Other researchers suggested that the growth reduction of η phase was caused by the aggregation of Si at the boundaries of grains and phases [22], the decrease of activity of aluminum [23], or the ternary phases acting as diffusion barriers [9].

Increasing Si content could reduce the melting point of aluminum alloys and increase the solubility of Fe in the liquid phase [32]. In addition, because the Si atoms preferentially diffused to the interface of dissimilar metals [22,29,33] and the solubility of Si in the η phase was relatively low, Fe−Al−Si ternary phase τ_1/τ_9 precipitated within the η phase with the further increasing Si content [34]. CHENG and WANG [31] considered that τ_1/τ_9 phase was formed by the reaction between the steel substrate and the η phase containing a solid solution of Si, which flattened the interface between steel and η phase. In the present research, the τ_1/τ_9 phase did not form a continuous layer (Figs. 4(c−d)). We deduced that the τ_1/τ_9 phase had an influence on the

growth kinetics of the η phase later in this work. When the Si content in the aluminum melt exceeded 5 wt.%, LEMMENS et al [9] observed the τ_5 phase in the reaction layers formed at 685 °C for 60 s. This indicated that more different ternary phases would form with time prolonging. Other researches [1,34] showed that Fe−Al−Si ternary phases were varied and had complex distribution. Thus, the effect of ternary phases on the interfacial reaction between solid steel and liquid aluminum should be investigated further.

With the increasing reaction time, the IMCs grew by the interfacial reaction, and more Fe atoms diffused to the aluminum melt. Therefore, the thickness of the η phase gradually increased and both the adhered θ phase and free θ phase gradually grew, as shown in Figs. 5(a, b) and Fig. 6.

The influence of temperature on the η phase was relatively complex. The results in Table 3 show that the η phase growth rate constant $K(T)$ increases with temperature increasing for the interfacial reaction of steel and pure aluminum, but the increment of $K(T)$ decreases at high temperature. The fitting value of $K(T)$ at 900 °C was lower than that at 850 °C for the reaction between steel and Al−2wt.%Si. These phenomena were attributed to the relatively high dissolution rate and solubility of Fe in the aluminum melt at high temperature. However, for higher Si contents the phenomena were not apparent. Previous research showed that the thickness of the η phase would almost remain unchanged when the growth and dissolution were balanced at high temperature [12]. Besides, the Si addition also made the solubility of Fe in the aluminum melt increase [32], and thereby prompted the dissolution of steel. When Si content was more than 5 wt.%, the thickness of IMCs was so small that the measurement error was large, which made the effect of dissolution not obvious. Moreover, CHEN et al [13] suggested that the order-disorder transformation of the η phase at high temperature would suppress the growth of the η phase. Because both the solubility and dissolution rate of Fe in the aluminum melt increased with increasing temperature, the steel dissolved sharply in the aluminum at high temperature. Thus, the θ phase increased with increasing temperature, as shown in Figs. 5(b, c). The growth mechanism of IMCs is complicated because it is influenced by the reaction temperature, reaction time, and Si content in the aluminum melt.

From the analysis above, the reaction between solid steel and liquid aluminum alloys could be divided into three modes in the initial reaction stage (0−10 s) at the temperature ranging from 700 to 900 °C, as shown in Fig. 11.

In the first mode, the steel reacted with the pure aluminum, as shown in Fig. 11(a). During the heating process, liquid aluminum wetted the surface of the steel, and Al atoms diffused into the solid steel. Then, the η phase nucleated and grew toward the steel side in a finger-like morphology. The dissolution process of IMCs had an obvious influence on the growth of η phase at high temperature. During the cooling process, Fe atoms diffusing into aluminum melt precipitated in the form of θ phase, which induced the formation of the serrated adhered θ phase and free θ phase in the aluminum substrate.

In the second mode, the steel reacted with the liquid Al−2wt.%Si, as shown in Fig. 11(b). During the heating process, the steel was wetted by the liquid Al−Si alloys. The Al atoms diffused into the solid steel, while Si atoms aggregated at the interface. Because Si suppressed the preferential growth of the η phase, the η phase nucleated and grew in a smooth wave-like morphology. Some Si atoms dissolved in the η phase. During the cooling process, more θ phases were formed.

In the third mode, the solid steel reacted with liquid Al−5wt.%Si and Al−8wt.%Si, as shown in Fig. 11(c). The enriched level of the Si atoms increased with the increasing Si content. The preferential growth of the η phase was almost suppressed. The thickness of η phase decreased obviously and the interface between η phase and steel flattened completely. At the same time, some Si atoms in the η phase precipitated in the form of punctate τ_1/τ_9 phase because the Si saturated solubility in the η phase was exceeded. In addition, the higher Si content led to the severer dissolution of the steel. During the cooling process, adhered θ phase and free θ phase increased and grew with increasing Si content.

4.2 Growth kinetics of η phase

The time exponent constant of the η growth kinetics is 0.77 in the initial stage of reaction between solid steel and liquid pure aluminum, as shown in Table 2. The result indicated that the

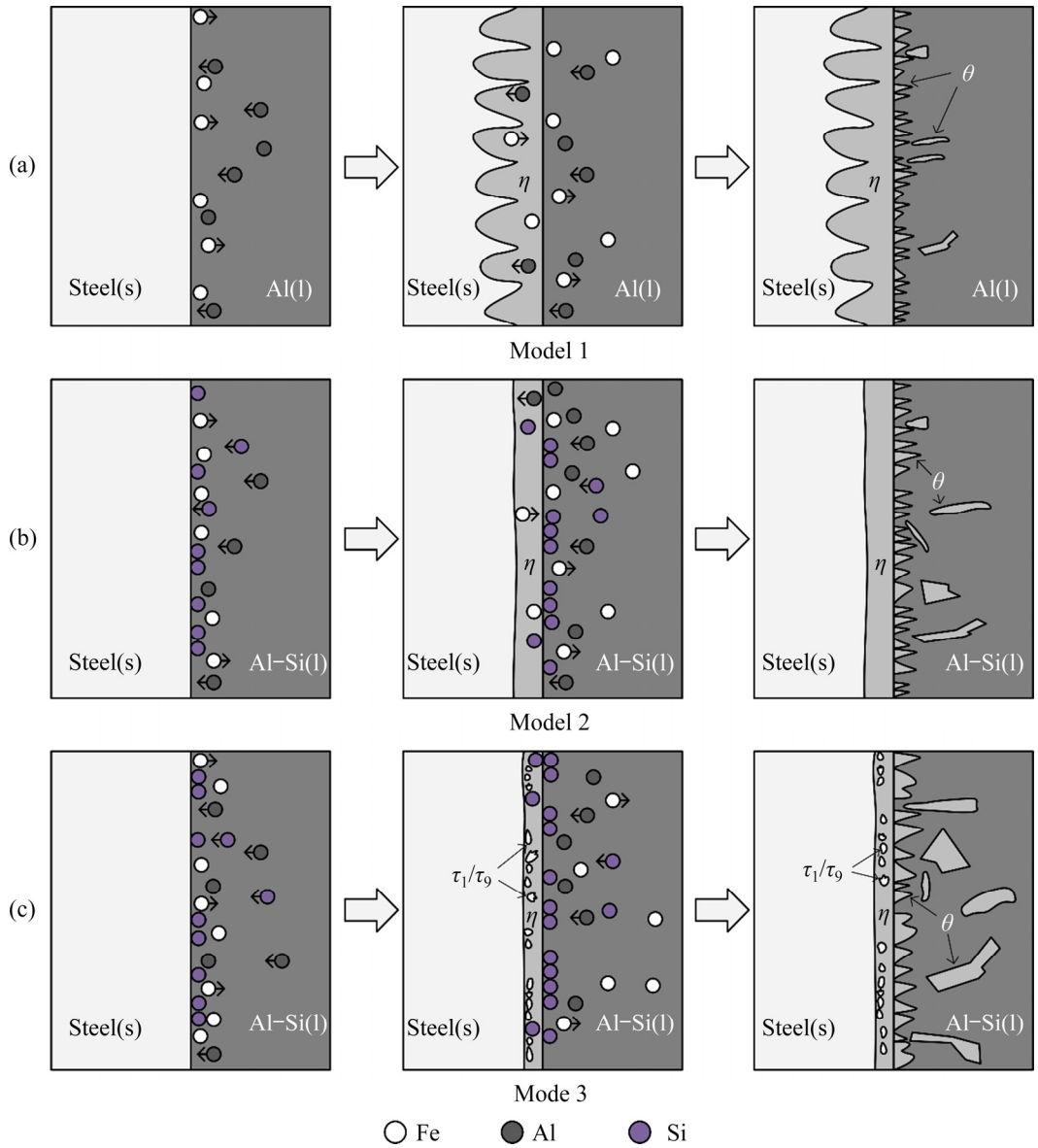

Fig. 11 Growth process of IMCs between solid steel and molten Al/Al−Si alloys in short time

growth of η phase average thickness was controlled by both the interfacial reaction and diffusion process. RONG et al [15] suggested that the growth along the *c*-axis of η phase was governed by the interfacial reaction, while the growth along other directions was governed by the diffusion process. Thus, the growth of η phase average thickness was governed by the interfacial reaction combined with the diffusion process. For longer reaction time, because the comparatively thick IMCs layers and some small-angle twist boundaries could hinder atoms diffusion [10,35], the diffusion process became the control mechanism of the η phase growth and then the growth obeyed a parabolic law.

When Si content in the aluminum melt was 2 wt.%, the time exponent was 0.52. This result indicated that the growth of the η phase was mainly governed by the diffusion process. Because the fast diffusion of Al atoms in the η phase was hindered by Si, the diffusion process became the dominant factor to suppress the growth of the η phase. Thus, the interface between η phase and steel in Fig. 4(b) presents a smooth morphology.

When Si contents in the aluminum melt reached 5 wt.% and 8 wt.%, the time exponents were respectively 0.76 and 0.86, as shown in Table 2. This result showed that the growth of the η phase was governed by both the interfacial reaction and diffusion process. Combining with analysis of the interfacial microstructures (Fig. 4), the reason

was as follows. When the solid solution of Si in the η phase reached a certain concentration, ternary phase τ_1/τ_9 preferentially formed. In the areas near the τ_1/τ_9 phase, the interfacial reaction forming η phase was suppressed by the reaction forming τ_1/τ_9 phase. Thus the growth of the η phase was mainly controlled by the interfacial reaction. In the areas away from the τ_1/τ_9 phase formation reaction, the growth of η phase was controlled by the diffusion process because of the suppression effects of Si on the atom diffusion process. Therefore, the growth of average thickness of the η phase was governed by the interfacial reaction combined with the diffusion process. When Si content in the aluminum melt was 8 wt.%, the time exponent n was higher than that when Si content was 5 wt.%. The higher concentration of Si might promote the formation of τ_1/τ_9 phase and further suppress the interfacial reaction forming the η phase. Previous researches showed that more kinds of ternary phases formed when the reaction time was longer [1,9]. These ternary phases might hinder the diffusion of the atoms by acting as diffusion barriers, and the growth of the η phase obeyed a parabolic law. The time exponent of η phase in Table 2 has an increasing trend with increasing temperature. The reason was that the increasing temperature increased the atom diffusion rates and thereby reduced the restriction of the diffusion process.

The partial data at high temperature in Fig. 7 are excluded in linear fitting, which is attributed to the increase of the dissolution rate. Because both the increasing temperature and the increasing Si content in the aluminum melt prompted the dissolution of Fe (mainly in the form of η phase), the dissolution process had a great effect on the kinetics calculation at high temperature. The growth kinetics of η phase was influenced by several factors such as measurement error, calculation error, and the dissolution of η phase in this work.

Table 5 shows that the value of E_a, namely the apparent activation energy of η, decreases with the increasing Si content, which is in accordance with previous research results [1,9,21]. From the trend of fitting lines in Fig. 7, when the temperature dropped to a certain level, the growth rate constant of η phase with 8 wt.% Si in the aluminum might be higher than that of η phase with 5 wt.% Si in the aluminum. Current research confirmed this phenomenon. SPRINGER et al [1] found that the η phase formed by the reaction between Al−5wt.%Si and steel was much thicker than the η phase formed by the reaction between pure aluminum and steel at 600 °C. LEMMENS et al [9] found that when Si content in the aluminum melt rose to 10 wt.%, the thickness of η phase gradually decreased with the temperature increasing from 670 to 725 °C. Moreover, ZHANG and LIU [36] suggested that the fast growth of IMCs at low temperature was related to the finer grain size and the faster grain boundary diffusion. Therefore, the phenomenon might be caused by the joint influence of increasing Si in the aluminum and the enhanced grain boundary diffusion.

4.3 Relationship between interfacial microstructure and mechanical properties

There was rougher fracture surface for the reaction of steel and pure aluminum filler metal case (Fig. 10(a)) than those of steel and Al−Si filler metals (Figs. 10(b−d)). Figure 9(b) shows that the impact energy of joint with pure aluminum filler metal is higher than that of joint with Al−Si filler metals. These indicated that the joint formed by the reaction between steel and pure aluminum filler metal had higher toughness.

In general, reducing the thickness of brittle IMCs was helpful to improve the performance of the Fe/Al joint [37]. In this research, the joint with pure aluminum filler metal had the thickest IMCs layer, but it had the optimum mechanical properties. We suggested that the unique finger-like morphology of the η phase induced good interfacial microstructures. The Fe-based solid solution with better toughness between η phase fingers suppressed effectively crack propagation. In addition, the solid solution of Si might lead to the poor mechanical properties of IMCs. The interface between steel and η phase exhibited smooth wave-like morphology when Si was added to the aluminum. The joint with Al−12wt.%Si filler metal had thinner IMCs layer but lower tensile strength than the joint with Al−8wt.%Si filler metal. This might be because a higher Si content in the aluminum melt induced the formation of more ternary phases in the IMCs, which reduced the mechanical properties of joints. SONG et al [32] found that the welding-brazing joint with Al−5wt.%Si filler metal had higher tensile strength than that with Al−12wt.%Si filler metal. They

suggested that when Si content in aluminum-based filler metal was 12 wt.%, the supersaturated solid solution of Si in the θ phase reduced the mechanical properties of IMCs.

Conclusively, the mechanical properties of joints formed by the reaction between low-carbon steel and aluminum-base filler metal were affected by the morphology, composition, and thickness of IMCs as well as the solid solution of Si in IMCs. In many applications related to the interfacial reaction between solid steel and molten aluminum, such as steel−aluminum brazing or welding−brazing, steel aluminizing, and bi-metallic manufacturing, Si was added in the aluminum to reduce the melting point of filler metal and the thickness of IMCs. However, this study showed that Si in the aluminum-based filler metal deteriorated the interfacial mechanical properties, although the thickness of IMCs decreased. Therefore, the effects of Fe−Al−Si ternary phases and the solid solution of Si in IMCs on the mechanical properties of joints should be taken into account when Si content in aluminum-based filler metal is relatively high.

5 Conclusions

(1) The reaction layers between steel and pure aluminum mainly consisted of the finger-like η phase adjacent to steel and the thinner serrated θ phase adjacent to aluminum. When Si content in the aluminum melt was 2 wt.%, the thickness of the η phase decreased and the interface between η and steel became smooth. When Si contents in the aluminum melt increased to 5 and 8 wt.%, τ_1/τ_9 phase formed in the η phase.

(2) The amount of IMCs increased with the increase of temperature and time. The dissolution process had an appreciable effect on the thickness of IMCs at high temperature.

(3) The growth of the η phase between steel and pure aluminum was governed by both the interfacial reaction and diffusion process at the temperature of 700−900 °C in the initial reaction stage. When Si content in the aluminum melt was 2 wt.%, the growth of the η was mainly controlled by the diffusion process. When Si contents in the aluminum melt were 5 and 8 wt.%, the growth of the η phase was governed by both the interfacial reaction and diffusion process. The apparent activation energy of the η phase decreased with increasing Si content.

(4) The joint with pure aluminum filler metal had higher mechanical properties than those with Al−Si filler metals. The joint with Al−8wt.%Si filler metal had the highest tensile strength among all the joints with Al−Si filler metals. When Si content is relatively high, the effects of more ternary phases and more solid solution of Si in IMCs might deteriorate the mechanical properties of Fe/Al joints.

Acknowledgments

The authors are grateful for the financial supports from the National Natural Science Foundation of China (No. 51875037), the Beijing Municipal Natural Science Foundation, China (No. 3192021), and the Fundamental Research Funds for the Central Universities, China (No. FRF-GF-18-004B).

References

[1] SPRINGER H, KOSTKA A, PAYTON E J, RAABE D, KAYSSER-PYZALLA A, EGGELER G. On the formation and growth of intermetallic phases during interdiffusion between low-carbon steel and aluminum alloys [J]. Acta Materialia, 2011, 59: 1586−1600.

[2] LI Yu-long, LIU Yan-ru, YANG Jin. First principle calculations and mechanical properties of the intermetallic compounds in a laser welded steel/aluminum joint [J]. Optics and Laser Technology, 2020, 122: 105875.

[3] ZHAO Hang, ZHANG Guo-tao, ZHANG Qing-xin, ZHANG Chao-qun, LI Yong-bing. Joining mechanism and mechanical properties of metallic bump assisted weld-bonded (MBaWB) joints of AA6061-T6 and bare DP590 [J]. Journal of Manufacturing Processes, 2020, 50: 204−215.

[4] MENG Yun-fei, GONG Meng-cheng, ZHANG Shuai, ZHANG Ya-zhou, GAO Ming. Effects of oscillating laser offset on microstructure and properties of dissimilar Al/steel butt-joint [J]. Optics and Lasers in Engineering, 2020, 128: 106037.

[5] YANG Jin, LI Yu-long, ZHANG Hua. Microstructure and mechanical properties of pulsed laser welded Al/steel dissimilar joint [J]. Transactions of Nonferrous Metals Society of China, 2016, 26: 994−1002.

[6] LIU Gui-qian, GAO Xiang-dong, PENG Cong, LIU Xiu-hang, HUANG Yi-jie, ZHANG Yan-xi, YOU De-yong. Tensile resistance, microstructures of intermetallic compounds, and fracture modes of welded steel/aluminum joints produced using laser lap welding [J]. Transactions of Nonferrous Metals Society of China, 2020, 30: 2639−2649.

[7] XUE Jun-yu, LI Yuan-xing, CHEN Hui, ZHU Zong-tao. Wettability, microstructure and properties of 6061 aluminum alloy/304 stainless steel butt joint achieved by laser-metal inert-gas hybrid welding-brazing [J]. Transactions of

Nonferrous Metals Society of China, 2018, 28: 1938−1946.
[8] CHENG Wei-jen, WANG Chaur-jeng. Growth of intermetallic layer in the aluminide mild steel during hot-dipping [J]. Surface & Coatings Technology, 2009, 204: 824−828.
[9] LEMMENS B, SPRINGER H, de GRAEVE I, de STRYCKER J, RAABE D, VERBEKEN K. Effect of silicon on the microstructure and growth kinetics of intermetallic phases formed during hot-dip aluminizing of ferritic steel [J]. Surface & Coatings Technology, 2017, 319: 104−109.
[10] DING Zong-ye, HU Qiao-dan, LU Wen-quan, GE Xuan, CAO Sheng, SUN Si-yu, YANG Tian-xing, XIA Ming-xu, LI Jian-guo. Microstructural evolution and growth behavior of intermetallic compounds at the liquid Al/solid Fe interface by synchrotron X-ray radiography [J]. Materials Characterization, 2018, 136: 157−164.
[11] KOBAYASHI S, YAKOU T. Control of intermetallic compound layers at interface between steel and aluminum by diffusion-treatment [J]. Materials Science and Engineering A, 2002, 338: 44−53.
[12] CHEN Shu-hai, YANG Dong-dong, ZHANG Ming-xin, HUANG Ji-hua, ZHAO Xing-ke. Interaction between the growth and dissolution of intermetallic compounds in the interfacial reaction between solid iron and liquid aluminum [J]. Metallurgical and Materials Transactions A, 2016, 47: 5088−5100.
[13] CHEN Shu-hai, YANG Da-wei, YANG Jian, HUANG Ji-hua, ZHAO Xing-ke. Nanoscale structures of the interfacial reaction layers between molten aluminum and solid steel based on thermophysical simulations [J]. Journal of Alloys and Compounds, 2018, 739: 184−189.
[14] TANAKA Y, KAJIHARA M. Kinetics of isothermal reactive diffusion between solid Fe and liquid Al [J]. Journal of Materials Science, 2010, 45: 5676−5684.
[15] RONG Ji-ping, KANG Zhi-fei, CHEN Shu-hai, YANG Da-wei, HUANG Ji-hua, YANG Jian. Growth kinetics and thickness prediction of interfacial intermetallic compounds between solid steel and molten aluminum based on thermophysical simulation in a few seconds [J]. Materials Characterization, 2017, 132: 413−421.
[16] YANG Jin, YU Zhi-shui, LI Yu-long, ZHANG Hua, GUO Wei, ZHOU Norman. Influence of alloy elements on microstructure and mechanical properties of Al/steel dissimilar joint by laser welding/brazing [J]. Welding in the World, 2018, 62: 427−433.
[17] CHEN Shu-hai, ZHAI Zhi-liang, HUANG Ji-hua, ZHAO Xing-ke, XIONG Ji-guang. Interface microstructure and fracture behavior of single/dual-beam laser welded steel-Al dissimilar joint produced with copper interlayer [J]. The International Journal of Advanced Manufacturing Technology, 2016, 82: 631−643.
[18] CAO R, CHANG J H, HUANG Q, ZHANG X B, YAN Y J, CHEN J H. Behaviors and effects of Zn coating on welding-brazing process of Al-steel and Mg-steel dissimilar metals [J]. Journal of Manufacturing Processes, 2018, 31: 674−688.
[19] ESMAILY H, HABIBOLAHZADEH A, TAJALLY M. Improving pulsed laser weldability of duplex stainless steel to 5456 aluminum alloy via friction stir process reinforcing of aluminum by BNi-2 brazing alloy [J]. Transactions of Nonferrous Metals Society of China, 2019, 29: 1401−1412.
[20] NICHOLLS J E. Hot-dipped aluminum coatings [J]. Anti-Corrosion Methods and Materials, 1964, 11(10): 16−21.
[21] YIN Fu-cheng, ZHAO Man-xiu, LIU Yong-xiong, HAN Wei, LI Zhi. Effect of Si on growth kinetics of intermetallic compounds during reaction between solid iron and molten aluminum [J]. Transactions of Nonferrous Metals Society of China, 2013, 23: 556−561.
[22] LEMMENS B, SPRINGER H, DUARTE M J, de GRAEVE I, de STRYCKER J, RAABE D, VERBEKEN K. Atom probe tomography of intermetallic phases and interfaces formed in dissimilar joining between Al alloys and steel [J]. Materials Characterization, 2016, 120: 268−272.
[23] ZHANG Kai, BIAN Xiu-fang, LI Yu-min, LIU Yang, YANG Chun-cheng. New evidence for the formation and growth mechanism of the intermetallic phase formed at the Al/Fe interface [J]. Journal of Materials Research, 2013, 28: 3279−3287.
[24] YANG Jin, HU An-ming, LI Yu-long, ZHANG Pei-lei, SAHA D C, YU Zhi-shui. Heat input, intermetallic compounds and mechanical properties of Al/steel cold metal transfer joints [J]. Journal of Materials Processing Technology, 2019, 272: 40−46.
[25] MA Hong, QIN Guo-liang, AO Zhi-yong, WANG Li-yuan. Interfacial microstructure and shear properties of aluminum alloy to steel fusion-brazed welded joint [J]. Journal of Materials Processing Technology, 2018, 252: 595−603.
[26] QIN Guo-liang, AO Zhi-yong, CHEN Yong, ZHANG Cun-sheng, GENG Pei-hao. Formability behavior of Al/steel MIG arc brazed-fusion welded joint [J]. Journal of Materials Processing Technology, 2019, 273: 116255.
[27] XIA Hong-bo, LI Li-qun, MA Nin-shu, TAN Cai-wang, GONG Jian-feng. Influence of energy ratio on dual-spot laser welded-brazed Al/steel butt joint [J]. Journal of Materials Processing Technology, 2020, 281: 116624.
[28] ZHANG C Q, LIU W. Non-parabolic Al3Ti intermetallic layer growth on aluminum-titanium interface at low annealing temperatures [J]. Materials Letters, 2019, 256: 126624.
[29] ZHANG Chao-qun, ROBSON J D, HAIGH S J, PRANGNELL P B. Interfacial segregation of alloying elements during dissimilar ultrasonic welding of AA6111 aluminum and Ti6Al4V titanium [J]. Metallurgical and Materials Transactions A, 2019, 50: 5143−5152.
[30] DU Yong, SCHUSTER J C, LIU Zi-kui, HU Rong-xiang, NASH P, SUN Wei-hua, ZHANG Wei-wei, WANG Jiong, ZHANG Li-jun, TANG Cheng-ying, ZHU Zhi-jun, LIU Shu-hong, OUYANG Yi-fang, ZHANG Wen-qing, KRENDELSBERGER N. A thermodynamic description of the Al−Fe−Si system over the whole composition and temperature ranges via a hybrid approach of CALPHAD and key experiments [J]. Intermetallics, 2008, 16: 554−570.
[31] CHENG Wei-jen, WANG Chaur-jeng. Microstructural evolution of intermetallic layer in hot-dipped aluminide mild steel with silicon addition [J]. Surface & Coatings Technology, 2011, 205: 4726−4731.
[32] SONG J L, LIN S B, YANG C L, FAN C L. Effects of Si additions on intermetallic compound layer of aluminum-steel

TIG welding-brazing joint [J]. Journal of Alloys and Compounds, 2009, 488: 217−222.
[33] XIA Hong-bo, ZHAO Xiao-ye, TAN Cai-wang, CHEN Bo, SONG Xiao-guo, LI Li-qun. Effect of Si content on the interfacial reactions in laser welded-brazed Al/steel dissimilar butted joint [J]. Journal of Materials Processing Technology, 2018, 258: 9−21.
[34] CHENG Wei-jen, WANG Chaur-jeng. Effect of silicon on the formation of intermetallic phases in aluminide coating on mild steel [J]. Intermetallics, 2011, 19: 1455−1460.
[35] SPRINGER H, SZCZEPANIAK A, RAABE D. On the role of zinc on the formation and growth of intermetallic phases during interdiffusion between steel and aluminium alloys [J]. Acta Materialia, 2015, 96: 203−211.
[36] ZHANG C Q, LIU W. Abnormal effect of temperature on intermetallic compound layer growth at aluminum-titanium interface: The role of grain boundary diffusion [J]. Materials Letters, 2019, 254: 1−4.
[37] LEMMENS B, SPRINGER H, PEETERS M, de GRAEVE I, de STRYCKER J, RAABE D, VERBEKEN K. Deformation induced degradation of hot-dip aluminized steel [J]. Materials Science & Engineering A, 2018, 710: 385−391.

Si 含量对固态钢/液态铝界面反应与界面力学性能的影响

邹天鹏[1]，喻高扬[1]，陈树海[1]，黄继华[1]，杨 健[1]，赵志毅[1]，荣吉平[1]，杨 瑾[2]

1. 北京科技大学 材料科学与工程学院，北京 100083；
2. 上海工程技术大学 材料工程学院，上海 201620

摘 要：采用热物理模拟方法研究 Si 含量对固态钢与液态铝界面反应初始阶段(反应时间<10 s)内金属间化合物的显微组织和生长动力学的影响。同时，通过高频感应加热的方式研究 Si 添加对钢/铝界面力学性能的影响。结果表明，在界面反应初期，金属间化合物层主要包括 η-Fe_2Al_5 和 θ-Fe_4Al_{13} 两相。铝液中添加 Si 后金属间化合物层的厚度减小。当 Al 液中含 2% Si(质量分数)时，η 相的生长仅由扩散过程控制；当铝液中 Si 含量增至 5%或 8%时，η 相的生长由扩散过程与界面反应共同控制，同时，τ_1/τ_9-$(Al, Si)_5Fe_3$ 三元相也在 η 相中形成。随着铝液中 Si 含量的增加，η 相的激活能逐渐减小。界面力学性能结果显示，纯铝与钢形成的接头具有最高的抗拉强度和冲击功。

关键词：金属间化合物；Si 含量；固态钢；液态铝；界面反应；力学性能

(Edited by Xiang-qun LI)